ARMY RESEARCH LABORATORY

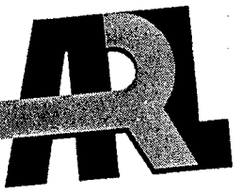

Image Segmentation of Hyperspectral Imagery

by Mark Wellman and Nassar Nasrabadi

July 2003

ARL-TR-2926

The findings in this report are not to be construed as an official Department of the Army position, unless so designated by other authorized documents.

Citation of manufacturers' or trade names does not constitute an official endorsement or approval of the use thereof.

DESTRUCTION NOTICE—Destroy this report when it is no longer needed. Do not return it to the originator.

Army Research Laboratory
Adelphi, MD 20783-1145

ARL-TR-2926 **July 2003**

Image Segmentation of Hyperspectral Imagery

by Mark Wellman and Nassar Nasrabadi

REPORT DOCUMENTATION PAGE

Form Approved

1. REPORT DATE (DD-MM-YYYY)	2. REPORT TYPE	3. DATES COVERED (From - To)
July 2003	Final	03/00–2/01

4. TITLE AND SUBTITLE
Image Segmentation of Hyperspectral Imagery

5a. CONTRACT NUMBER

5b. GRANT NUMBER

5c. PROGRAM ELEMENT NUMBER

6. AUTHOR(S)
Mark Wellman and Nassar Nasrabadi

5d. PROJECT NUMBER
61120

5e. TASK NUMBER

5f. WORK UNIT NUMBER

7. PERFORMING ORGANIZATION NAME(S) AND ADDRESS(ES)
U.S. Army Research Laboratory
Sensors & Electron Devices Directorate
(ATTN: AMSRL-SE-SE) mwellman@arl.mil

8. PERFORMING ORGANIZATION REPORT NUMBER
ARL-TR-2926

9. SPONSORING/MONITORING AGENCY NAME(S) AND ADDRESS(ES)
U.S. Army Research Laboratory
2800 Powder Mill Road
Adelphi, MD 20783-1145

10. SPONSOR/MONITOR'S ACRONYM(S)

11. SPONSOR/MONITOR'S REPORT NUMBER(S)

12. DISTRIBUTION/AVAILABILITY STATEMENT
Approved for public release; distribution unlimited.

13. SUPPLEMENTARY NOTES
Hyperspectral, segmentation, feature extracts

14. ABSTRACT

Hyperspectral imagery (HSI), a passive technique creating a large collection of images of fine resolution across the infrared spectrum is currently being considered for U.S. Army tactical applications. An important tactical application of infrared (IR) hyperspectral imagery is the detection of low-contrast targets, including those targets that may employ camouflage, concealment, and deception (CCD) techniques [1, 2]. Spectral reflectivity characteristics were used for efficient segmentation between different materials such as painted metal, vegetation, and soil for visible to near IR bands in the range of 0.46–1.0 μm as shown previously by Kwon et al. [3]. We are currently investigating the HSI region spanning the wavelengths from 7.5 to 13.7 μm. The energy in this range of wavelengths is almost entirely emitted rather than reflected; therefore, the gray level of a pixel is a function of the temperature and emissivity of the object. This is beneficial because light level and refection will not need to be considered in the segmentation. We will present results of segmentation analysis on the long-wave infrared (LWIR) hyperspectrum using a simple distance metric applied to full-band and sub-band HSI data sets, neural network-based classification approaches, and principal component analysis (PCA) applied to relative temperature profiles derived from the Spatially Enhanced Broadband Array Spectrograph System (SEBASS) database. A stepwise segmentation will be demonstrated using a back-propagation neural network, which outlines some of the difficulties in the multi-class case. Overall, these results should give an early indication of the added capability hyperspectral imagery and algorithms will bring to bear on the target acquisition problem.

15. SUBJECT TERMS Hyperspectral, Segmentation, Feature Extracts

16. SECURITY CLASSIFICATION OF:			17. LIMITATION OF ABSTRACT	18. NUMBER OF PAGES	19a. NAME OF RESPONSIBLE PERSON
a. REPORT	b. ABSTRACT	c. THIS PAGE			Mark Wellman
UNCLASSIFIED	UNCLASSIFIED	UNCLASSIFIED	SAR	45	19b. TELEPHONE NUMBER (*Include area code*) (301) 394-2165

Standard Form 298 (Rev. 8/98)
Prescribed by ANSI Std. Z39

Contents

Figures

Tables

1. Introduction

Hyperspectral imaging has found wide usage in the remote sensor community and more recently, we have seen a branching out into the commercial (crop health monitoring and food management for example) and the medical arena. One exciting medical research application is the use of hyperspectral techniques to map functional areas of the brain. In military applications, hyperspectral data can detect chemical and biological agents, penetrate foliage to detect troops and vehicles, lead to the creation of improved, smart missile seekers and serve as a countermeasure against ground targets, employing camouflage and concealment techniques. Segmentation of HSI data is normally based on discrimination between materials using the spectral signature in thermal emissions or solar reflectance [3]. It is also important to reduce the data volume and dimensionality without loss of discrimination. Many methods have been attempted in the past; Harsanyi and Chang [4] used an orthogonal subspace projection approach, projecting each HSI pixel vector onto a subspace that is orthogonal to undesired signatures. In this report, we will present results using a similar and simpler technique, generating the "principal" components for unknown HSI pixel vectors using only target eigenvectors followed by segmentation of the image.

H. Kwon et al. [3] used mean spectral band curves of HSI pixels for different materials and developed an adaptive segmentation technique with reduced computational cost. Rauss et al. [5] employed another adaptive technique, genetic programming that had two advantages; first, no assumptions were needed about the character of the HSI data and secondly, genetic programming results elaborate which spectral bands are most useful for discrimination. The joint band prioritization and decorrelation approach by Chang et al., demonstrated that in some cases, over 90% of the total HSI spectral bands could be removed without loss in discrimination [6].

1.1 Hyperspectral Imagery and Preprocessing

One tactical application that is our primary concern for investigation is the detection of low-contrast thermal targets using the LWIR region extending from 7.5 μm to 13.7 μm.

In Figure 1, we have an LWIR broadband image of interest. This image is the summation of all radiance values across the spectral range for each pixel. Images like this example were used to derive a feature space for the target, tree and ground radiometric data for 128 spectral bands (7.5 – 13.7 μm) of interest within one pixel.

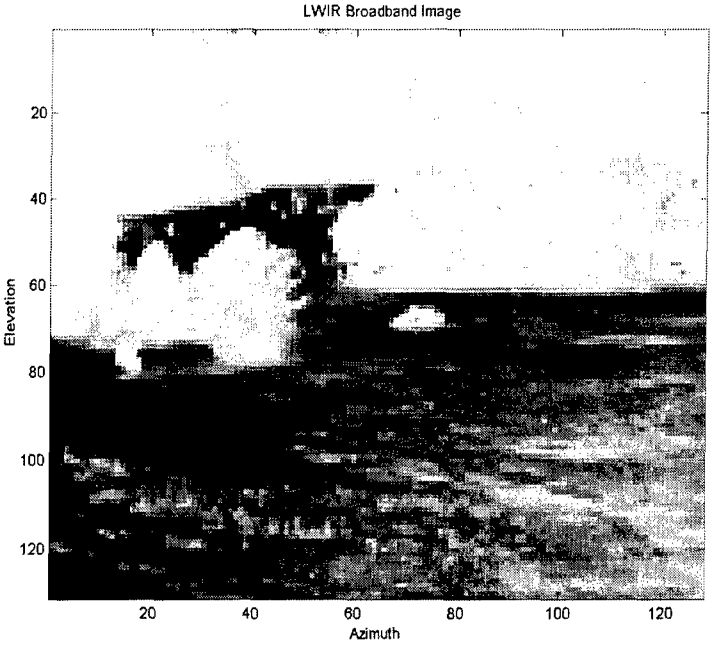

Figure 1. LWIR Summation of RD7 image. A M60 tank is close to the center.

Earlier work in our group and others [1–3, 5] showed that it was useful to convert the radiometric SEBASS data to apparent temperature using the relationship:

$$T_{App} = \frac{hc}{k\lambda \log\left(\frac{2c}{\lambda^5 Q} + 1\right)}$$

with Q in Watts/cm^2, λ the wavelength and h, c, and k constants. (1)

One can readily see the distinction present when comparing radiance to relative temperature. The plots in Figure 2 were taken from the same pixel location for a target of interest. The slight depression in the spectral radiance plot near 9 μm is far more obvious in the relative temperature profile. These slight differences in shape characteristics can be exploited for segmentation and classification of materials once the inherent "black-body" curve is removed from the radiance measure, thus the utility of conversion to relative temperature.

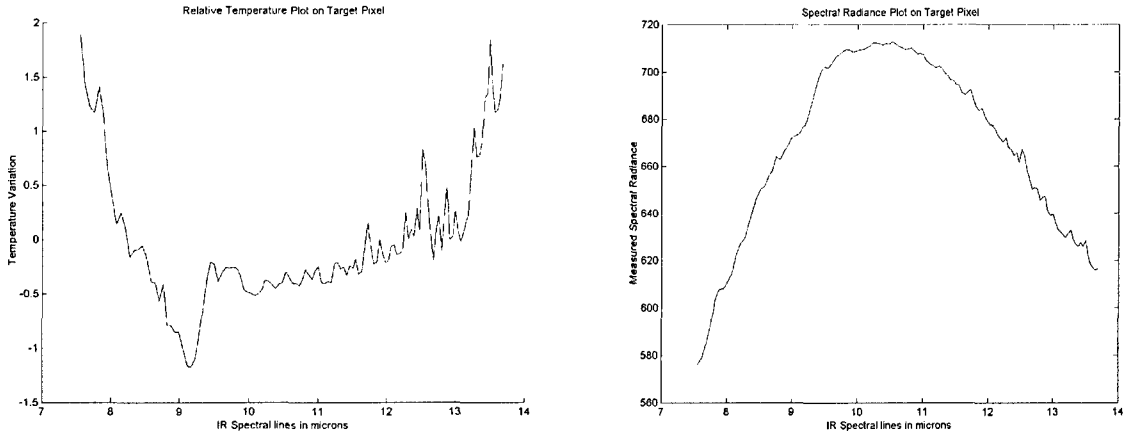

Figure 2. The left image is a relative temperature plot for a U.S. target pixel and on the right, the radiance plot for the same pixel location.

2. Feature Extraction

We can consider equation (1), a feature extraction processing step with the resulting relative temperature profile representing the new feature space. Fundamentally, the feature extraction process involves choosing a set of features for a class of patterns that will exhibit and maintain class separability under the constraint of some criterion function. Typically, feature extraction is considered a mapping from an m-dimensional space, to a smaller subspace n and here we can consider the removal of the redundant feature, the "black-body" curve as a reduced feature space. Further reduction in the dimension of the feature space can be accomplished by various means.

Consider the following set of relative temperature curves for the various classes we will investigate.

In Figure 3, we see some of the variety in the relative temperature profiles for each class. Take notice of the sharp depression in the U.S. target and exposed ground class, or the broad sweeping depression, slightly shifted toward longer wavelengths in the foreign target case.

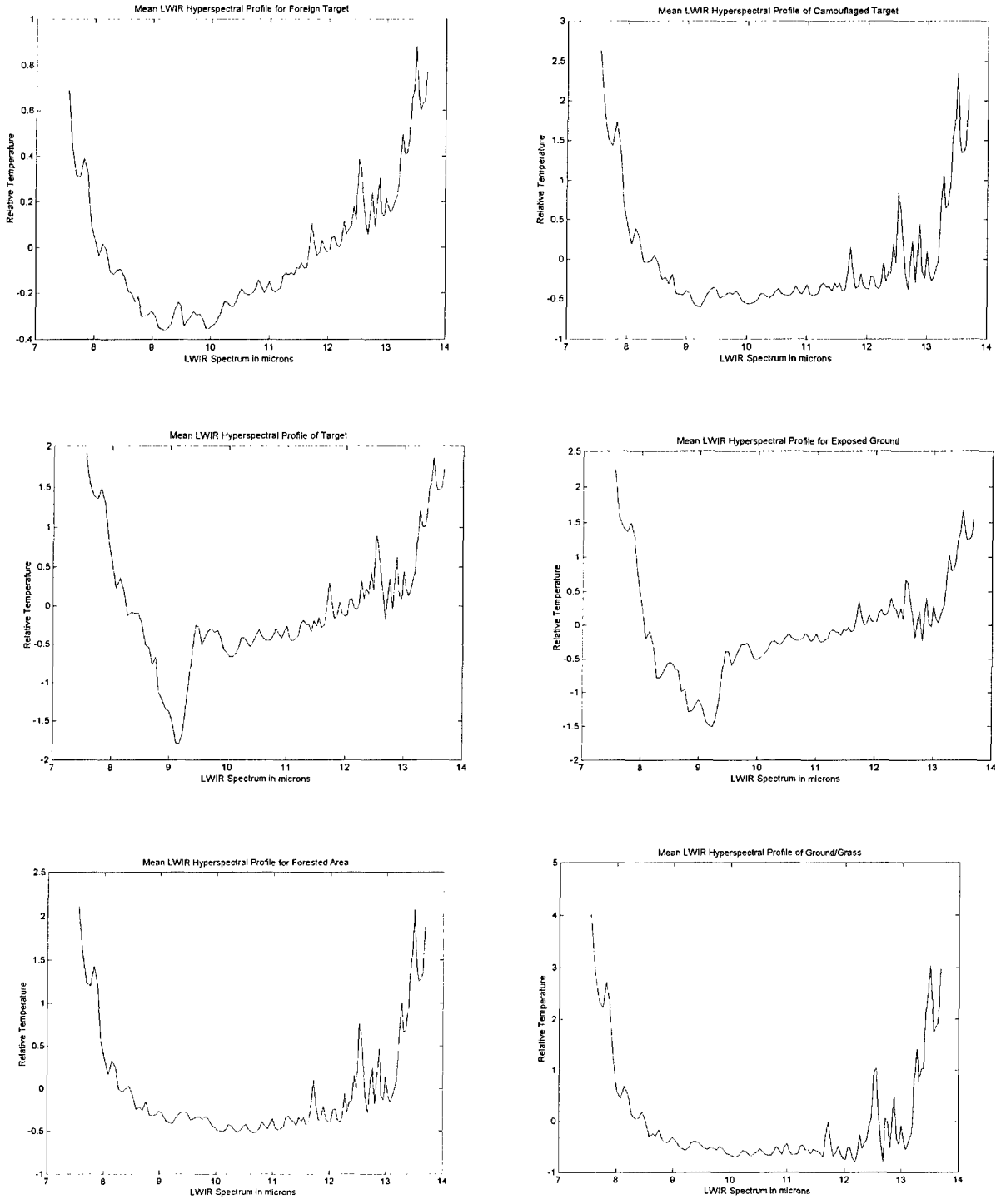

Figure 3. The relative temperature plots for the 6 classes of target/clutter considered in the paper.

2.1 Broadband, Narrowband and Sub-Band Features

One feature extraction and segmentation method to consider is using comparisons of features derived from narrow-band and/or broadband ratio and difference characteristics in the relative temperature profiles. Broadband ratios, chosen carefully, should yield a feature or set of features that allow discrimination using simple techniques for the target and foreign target and to some degree, discriminating exposed ground in the presence of the remainder of the classes. Exposed ground has been a difficult issue for segmentation because it closely resembles target signatures. Take notice in Figure 3 of the foreign target spectrum and the broad depression from 8 to 11 μm, and compare this to the narrow depression exhibited by the U.S. target. A broadband ratio could be used in this case. As an example, calculate the ratio of the relative temperature from 8.5–9.5 μm and 9.5–10.5 μm. Although as can be seen, the "exposed" ground will confuse the issue with the target if this were the only feature considered. Further feature extraction can be accomplished by using narrow-band ratios or narrow-band differences [7]. Consider the exposed ground spectral plot; in all cases, we see a pronounced depression in the area slightly >8 μm. A good narrow-band difference feature is the difference between relative temperature profiles at 8.5788 and 8.2706 μm. This difference can be far more pronounced for other exposed ground pixels. Camouflage HSI signatures present another problem. Often, we see mixed pixels, which do not lend themselves to segmentation although some detection is possible. Simple pixel identification is probably not sufficient for segmentation of camouflage targets. Sub-banding is simply selecting regions of the relative temperature profiles for segmentation purposes that exhibit less redundancy over the range of wavelengths. This has proven to be useful in past research as well [1] and may give some immunity to diurnal variations. We will revisit this topic later in the paper.

2.2 Principal Component Analysis

Another feature extraction method that holds promise is principal component analysis (PCA) and has been used for band selection of multi-spectral imagery [8] in the past. PCA is also regarded as a decorrelation technique widely used in data compression and interpretation. This technique exhibits a high degree of energy compaction; it transforms the original feature space into an uncorrelated space, thus, you gain the advantage of reduced complexity in your segmentation/classification architecture due to the reduced dimension of the feature space. Principal components are derived from the following set of relationships: Let $\mathbf{u}$, defined as

$$\mathbf{u} = [u(\omega_1), u(\omega_2), \ldots\ldots u(\omega_N)]^T, \tag{2}$$

be an N x 1 random input vector and assume zero mean without loss of generality. Let $\mathbf{R}$, be the N x N correlation matrix of the data with eigenvalues $\lambda_1, \lambda_2, \ldots, \lambda_N$. The k principal components are defined by the linear transformation,

$$\mathbf{C} = \Phi^T \mathbf{u}, \tag{3}$$

where $\mathbf{C} = [c_1, c_2, ..., c_k]^T$ is a k x 1 principal component matrix, and Φ is an N x k matrix, with columns corresponding to the k eigenvectors for the k largest eigenvalues of $\mathbf{R}$. We can choose the value for k arbitrarily, where k is significantly smaller than N, thus reducing the feature space and in some cases, retaining separability.

We hope to exploit PCA with an appropriate classifier architecture in the segmentation of the various classes and targets. Figure 4 includes a plot of the magnitudes for the first six eigenvalues associated with the target, tree and ground pixels from the HSI training set. The magnitudes of the 2nd, 3rd and 4th for the three classes is of special importance. The projection of a test pixel (principal components) onto the eigenspace of the target could be beneficial.

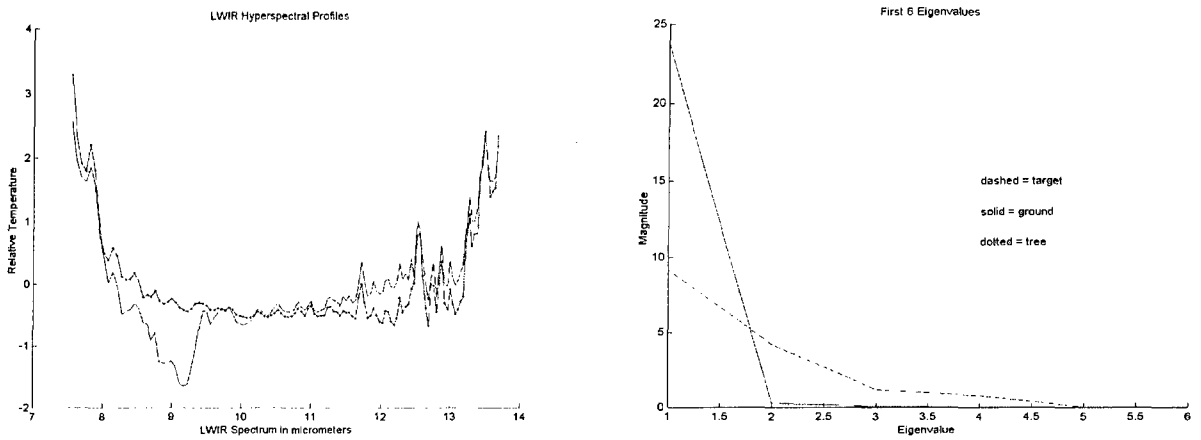

Figure 4. The relative temperature plot on the left displays U.S. target in solid line, the tree clutter in dot/dashed line, and the ground/grass clutter in dashed line.

The LWIR spectrums, similar to those in Figure 4 are projected into the target eigensubspace with the resulting projections passed into neural network for discrimination.

In Figure 5, we see eight feature components being formed by the process and then passed to the trained neural network for discrimination.

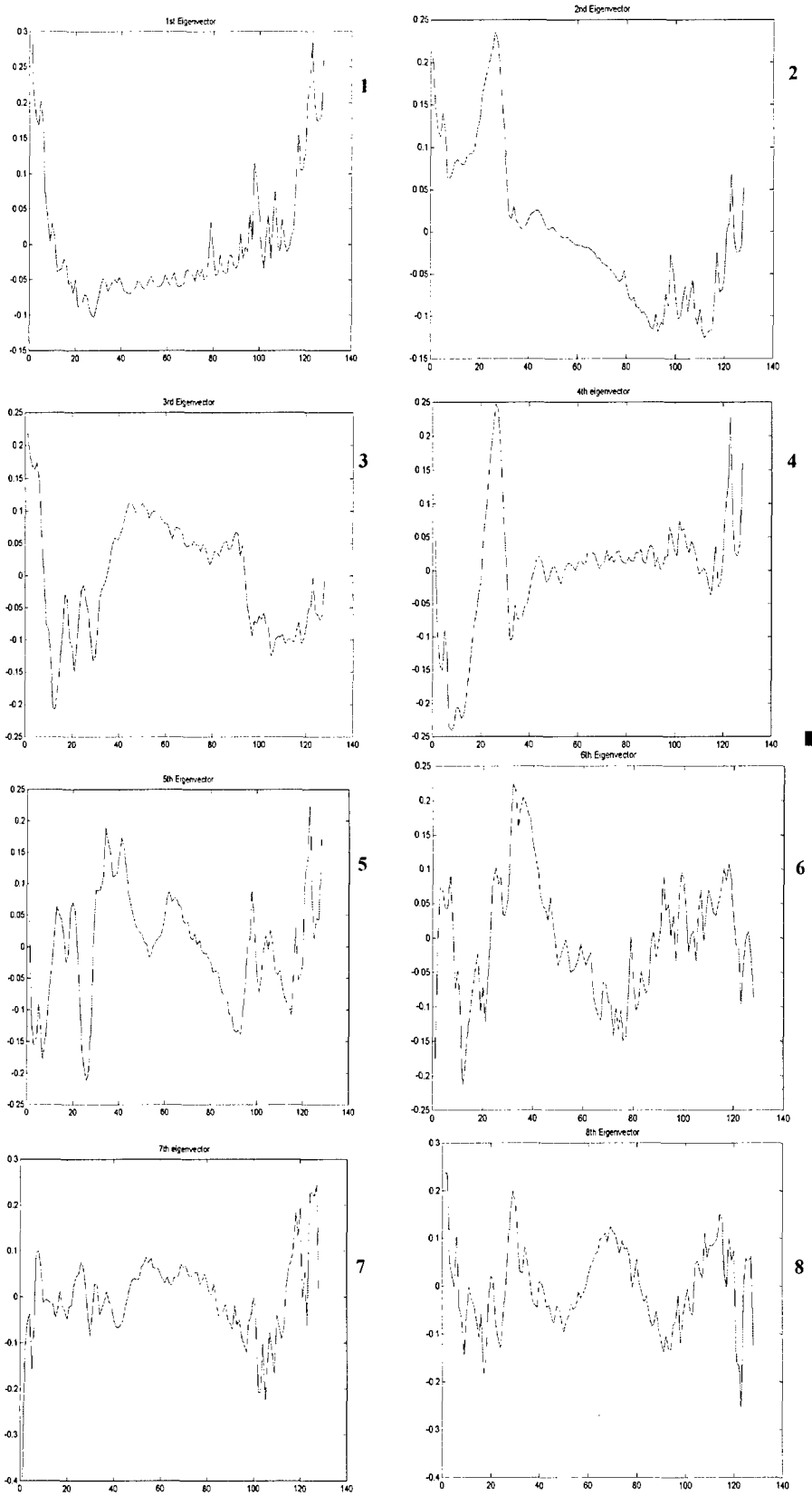

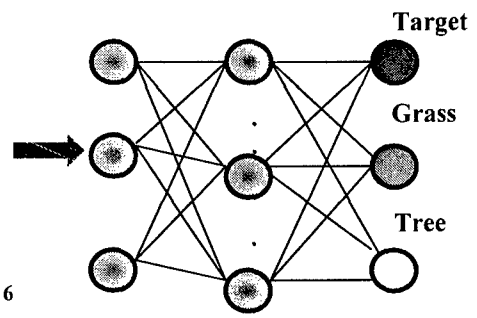

Figure 5. The projection process using eigenvectors derived from target.

3. Segmentation Techniques

We have addressed the feature extraction and optimization problem somewhat, but the caveat to the problem at hand is in the selection of an appropriate classifier topology for efficient segmentation. Excellent features would be amenable to any type of classifier topology [9], but the multi-dimension nature of the HSI space may require one to consider classifiers that can parse the feature space efficiently. We will not consider parametric architectures, although it may prove that a model with statistical parameters fitting the HSI space has exceptional performance. This is an avenue we may take in the future. Non-parametric and boundary decisions classifier topologies are able to model statistical distributions that are highly non-Gaussian and/or multi-modal in nature, and past work has pursued these somewhat. We will employ these architectures.

In coarse observation of the relative temperature profiles in Figure 6, distinctions are readily apparent, which may allow very simple segmentation techniques to be employed. The integration of specific spectral regions could prove valuable, also, distance metrics should be able to take advantage of the apparent differences as seen when comparing target profiles to grass and ground in the regions from 8.0 to 10.0 μm and the region from 11.0 to 12.6 μm.

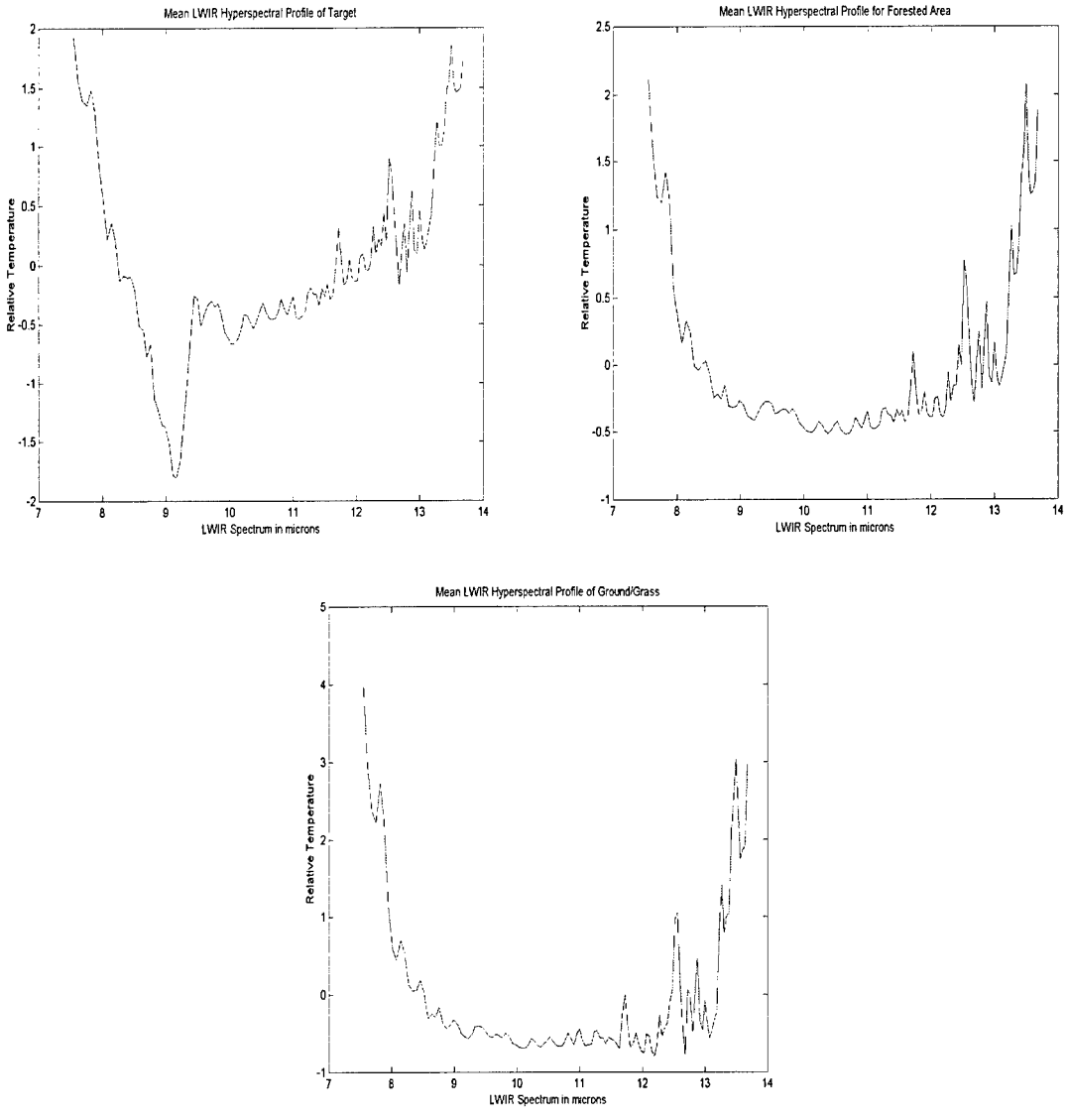

Figure 6. From left to right, target, tree and grass/ground mean relative temperature plots.

3.1 Simple Segmentation Algorithms

Euclidean distance between two patterns, $\mathbf{X}$ and $\mathbf{Z}$,

$$D = \|\mathbf{X} - \mathbf{Z}\|, \tag{4}$$

is one measure of similarity.

Figure 7 demonstrates a full-band segmentation result using an Euclidean distance measure.

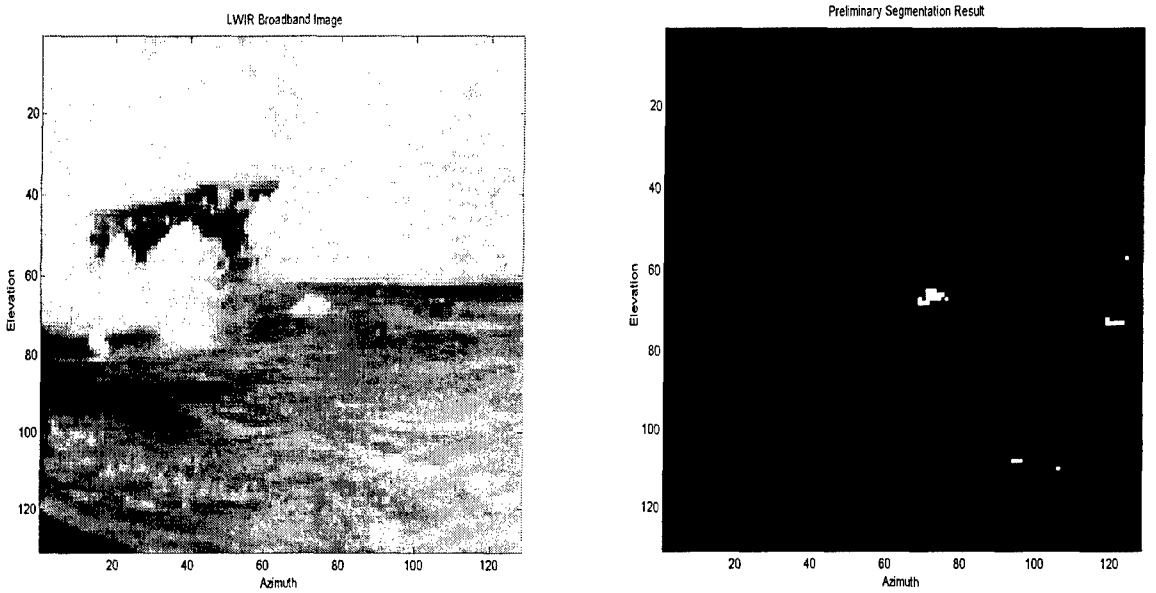

Figure 7. On the right, we have a segmentation result using all 128 bands for the distance metric.

In comparing the summation image and the segmented image of Figure 7, our two class (target, background) segmentation was quite effective and preliminary results are very promising. However, the problem becomes much more difficult when considering the various camouflage, concealment and deception methods, diurnal effects and simple placement of the target within a tree line. Also, the ground pixel relative temperature profiles are richer in diversity and required an expansion of our training database. These factors dictate the need to consider alternative segmentation methods.

Several useful distance measures can be of benefit when considering statistical properties of the HSI patterns. The Mahalanobis distance is given by

$$D = (\mathbf{X}-\mathbf{M})^T \, \mathbf{C}^{-1} (\mathbf{X}-\mathbf{M}), \tag{5}$$

with $\mathbf{C}$; the covariance matrix of the pattern population $\mathbf{M}$ as the mean vector, and $\mathbf{X}$ as the unknown pattern, have been useful in the past but their performance relies on the underlying class distribution [7] being nearly multivariate Gaussian. Also, the inverse of the covariance matrix must

be estimated from the eigendecomposition; direct estimation is impossible due to the "ill-conditioned" nature of covariance matrix. Another measure that has been useful in taxonomy and information retrieval is the so-called "Tanimoto measure," given by

$$S(\mathbf{X},\mathbf{Z}) = \frac{\mathbf{X}^T\mathbf{Z}}{\mathbf{X}^T\mathbf{X} + \mathbf{Z}^T\mathbf{Z} - \mathbf{X}^T\mathbf{Z}} \tag{6}$$

with known pattern vector $\mathbf{Z}$, is maximized when the cross-correlation is maximum. Non-metric similarity estimates also exist which measure the orientation in multidimensional space and are of benefit when classes develop along principal axes [10]. One such method is the cosine of the angle between the unknown vector $\mathbf{X}$ and the pattern vector $\mathbf{Z}$ given by

$$S(\mathbf{X},\mathbf{Z}) = \frac{\mathbf{X}^T\mathbf{Z}}{\|\mathbf{X}\|\,\|\mathbf{Z}\|}, \tag{7}$$

and is maximized when the unknown vector and pattern vector are oriented in the same direction with respect to the origin.

3.2 Gaussian Mixture

A powerful non-parametric classifier we adopted for some preliminary test was the Gaussian mixture architecture. The Gaussian mixture classifier is a refinement of the multivariate Gaussian technique and is considered a nonparametric technique because one will use the data to generate the mixed Gaussians. In this case, the probability distributions are modeled as a weighted set of Gaussians. The conditional distributions are given by

$$p(X/c_j) = \sum_{k=1}^{Ng} w_k G_k \tag{8}$$

with w_k, the weight of the k-th Gaussian G_k and the weights sum to one. The Gaussians are given by

$$G_k = \frac{1}{(2\pi)^{n/2}|R_k|^{1/2}} \exp\left(-\frac{1}{2}(X - M_k)^T R_k^{-1}(X - M_k)\right) \tag{9}$$

with R_k, the covariance matrix for the kth Gaussian, and M_k as the corresponding mean vector. Training is accomplished using an iterative procedure known as the estimate-maximize algorithm [11], which maximizes the likelihood of the training set generated by the probability distribution function. The parameters estimated are simply the weights, mean vectors and covariance. See references [12] and [13] for the training procedure. Table 1 has a preliminary classification result using a Gaussian mixture architecture. In future work, we will investigate this architecture further as well as other techniques.

Table 1. The values in the table represent the percentage of pixels classified using cross-validation with correct classification along the main diagonal.

Gaussian Mixture (%)

	target	tree	ground
target	86	0	0
tree	14	99	10
ground	0	1	90

3.3 Boundary Decision Architectures

There are several boundary decision architectures available; for example, the simplest and most often used is the back-propagation neural network (BPNN), which allows for separation of complex hyperboundaries depending on the number and size of the hidden layers. We have employed the BPNN with an adaptive learning rate that allows fine-grain adjustments during training. Smoothing is also incorporated and allows the control of weight adjustment based on the past values of gradient descent and can prevent the training process from terminating in shallow local minimum [14]. For target identification and segmentation, the BPNN can provide both a robust classifier and a measure of your confidence in the classification decision. BPNNs' derive their computational power from the parallel-distributed structure and the ability to learn and adapt. Specifics governing the neural network training flow are beyond the scope of this paper. We will present several results using the BPNN for segmentation in later sections of the paper.

4. Hyperspectral Database

SEBASS HSI hypercubes were radiometrically calibrated [7] and the resulting 3-dimensional (3-D) cubes were used for developing our database. The calibrated hypercubes are $128(\lambda) \times 131 \times 128$ with 128 individual bands ranging from 7.5466 to 13.6772 μm and bandwidths from 0.0691 to 0.0368 μm. The relative temperature training database we constructed consists of U.S. and foreign target pixels where both open terrain and CCD targets are represented. The tree, ground and exposed ground pixels were selected arbitrarily but with great care in parsing them after initial selection to remove outliers or what may be considered as mixed pixels. This procedure though is very subjective and represents a problem for the camouflaged cases. The training pixels of all classes also represent a cross section of the HSI images from 5:00 am to 8:00 pm; however, a set of hypercubes where "temperature inversion" is observed was not included.

4.1 Ground Truth

In order to render the images for viewing, a summation of all radiance values across the LWIR spectrum was performed (Figure 8).

These are the representative scenes we have considered in our work. Both are very rich in diversity with respect to the relative temperature profiles for various targets. In Figure 8, both scenes have several targets of interest and clutter. Target and type are located at the following positions for RD7XXXX files.

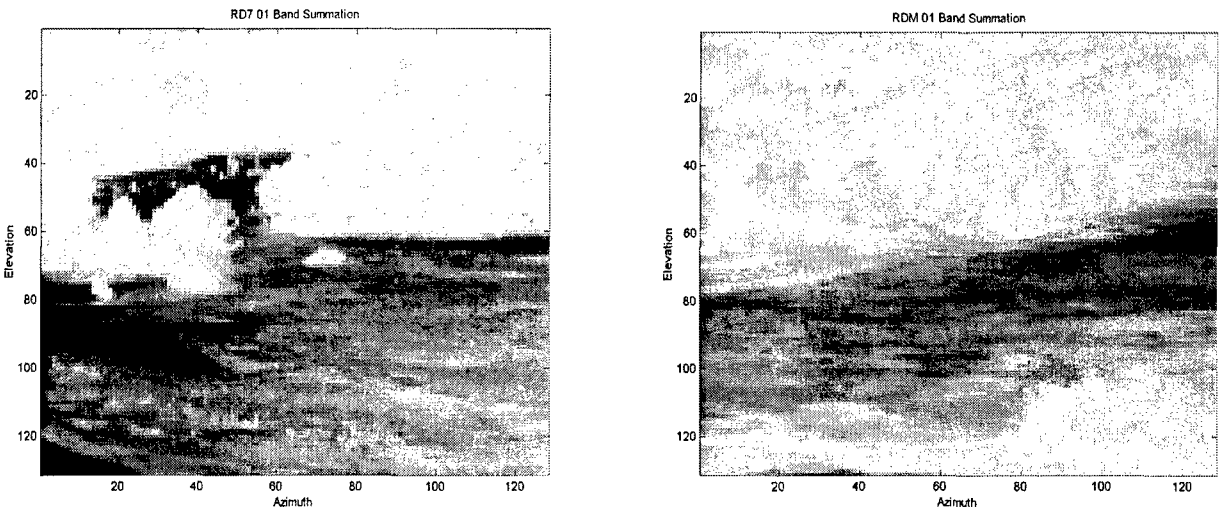

Figure 8. Summation images for RD7 and RDM cases.

Azimuth	Elevation	Target
X 72	Y 64	M60 NETTING NONE
X 84	Y 55	T72 NETTING NONE
X 122	Y 53	ZIL131 NETTING NONE
X 28	Y 68	BTR70 NETTING NONE

The M60 is readily apparent in the center of the image, see Fig. 8, left-hand side.

The RDMXXXX files have targets located as follows but with large tracts of exposed ground filling several areas of the image as well.

Azimuth	Elevation	Target
X 2	Y 63	M2 NETTING NONE
X 54	Y 59	M1 NETTING LCSSWOOD

The M2 is near the left border and the summation image indicates something unusual at this position.

4.2 Characteristic Hyperspectral Imagery

The following images in Figure 9 exhibit several of the characteristic renderings for the two regions of interest in this paper. One should compare the band summation directly with the band-subtraction results, which was shown to be useful in detecting some CCD targets by various researchers [2, 7]. The band-subtraction was performed by subtracting the radiance values at 10.77 μm and 9.97 μm.

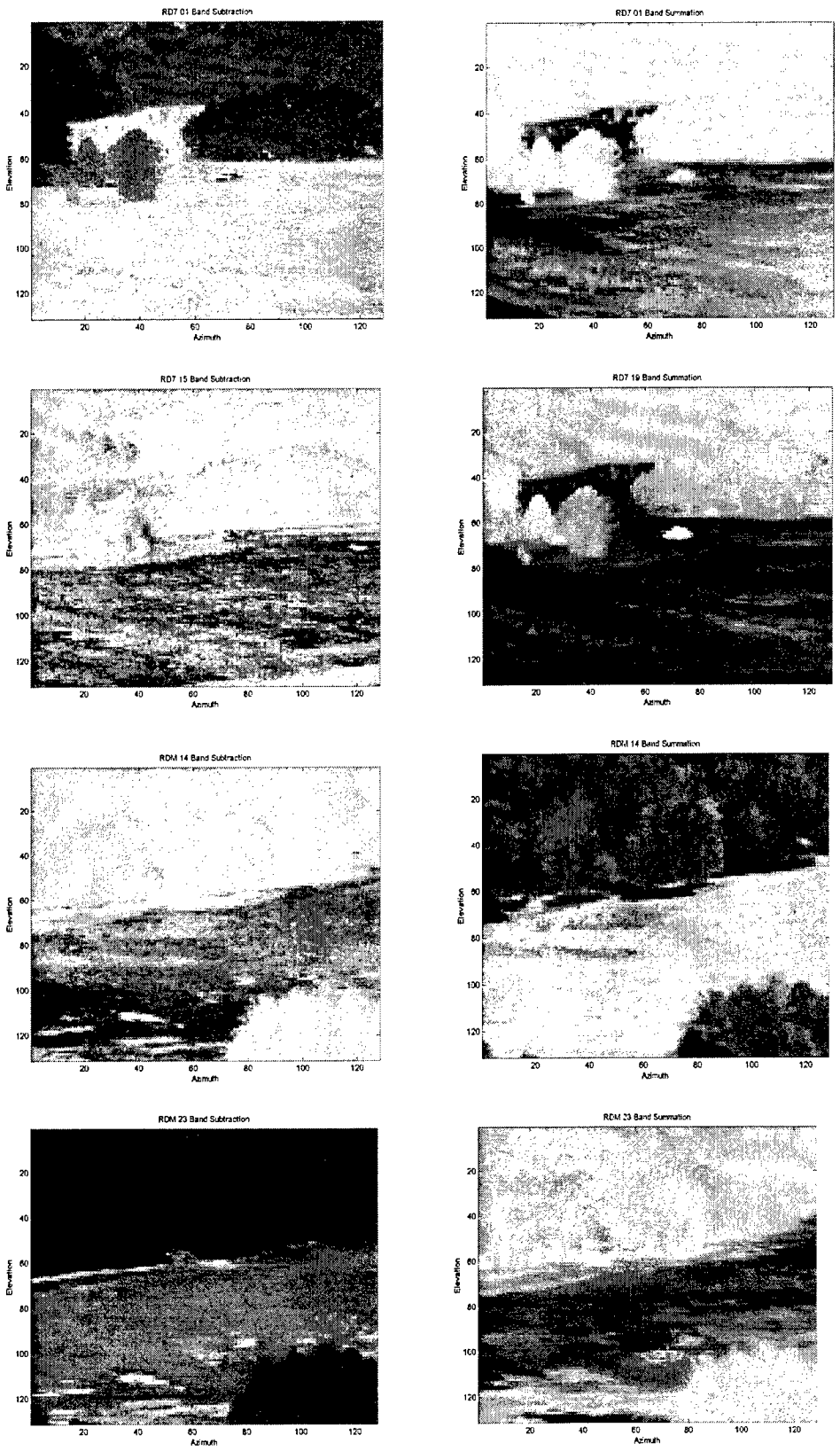

Figure 9. Band subtraction and band summation images for RD7 and RDM cases.

On close inspection of the RDM images, one can see the camouflaged target sitting at elevation 59 and azimuth 54. Band summation fails to distinguish any target presence and is similar to what the naked eye may determine; however, band-subtraction suggests the presence of something unusual sitting in the group of trees. Band subtraction suggests that other narrow band features may be of utility in discriminating various classes. A goal is to further bring out the features in the RDM image group, especially the camouflage target.

5. Segmentation Results

We present the stepwise segmentation on full-band, relative temperature images using the BPNN as our choice for classifier architecture. Each subsection will be devoted to particular subset of classes.

5.1 Segmentation of 3 Classes Using BPNN

The 8 images of Figure 10 demonstrate the result of segmentation for the 3-class case using the trained BPNN. The 3 class case only includes tree, ground/grass and U.S. target (Figure 3) We see that we can clearly discriminate the target from the background in the RD7 case, but the exposed ground present in the RDM case greatly obscures the result. The relative temperature profiles for exposed ground are very similar to the U.S. target pixels chosen for training. In some instances, we detect something in the tree line for RD7, and we can distinguish the M2 target at azimuth = 2 and elevation = 63 in the RDM cases, but the camouflaged M1 is completely invisible to the segmentation, and the resulting confusion of the exposed ground must be addressed. The full spectrum performs well for the simple case but suffers in the camouflaged case. In RDM 23, we can detect a portion of the target but the "false" alarms are too great. The RD715 and RDM14 results are due to "temperature inversion" and we will see several cases of this problem in other segmentation results.

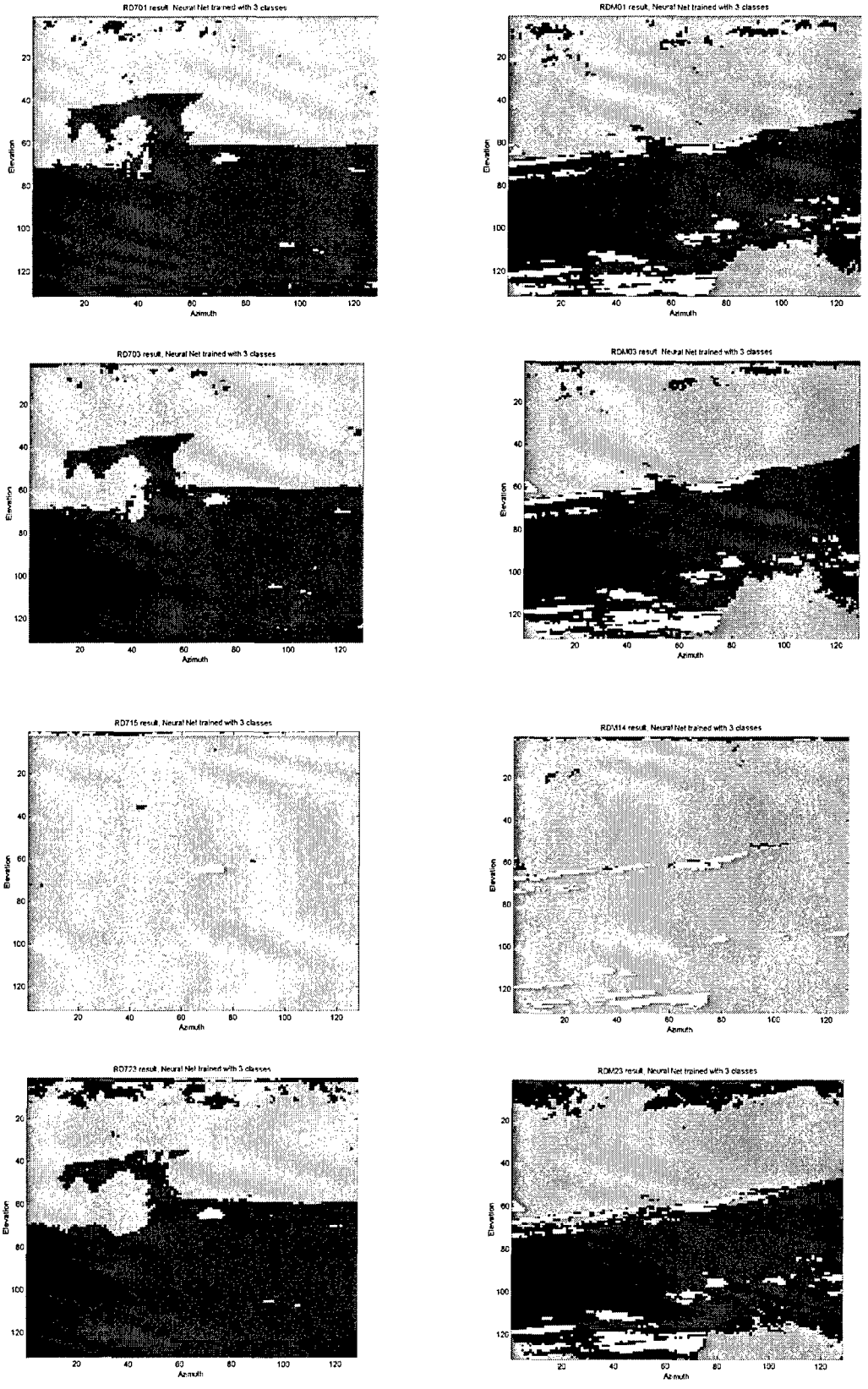

Figure 10. RD7 and RDM segmentation results using a BPNN, trained with only the 3 classes, U.S. target, tree and grass/ground.

5.2 Segmentation 4 Class Using BPNN

Let us add the exposed ground class to the problem. What follows in Figure 11 are the results for the 4-class segmentation.

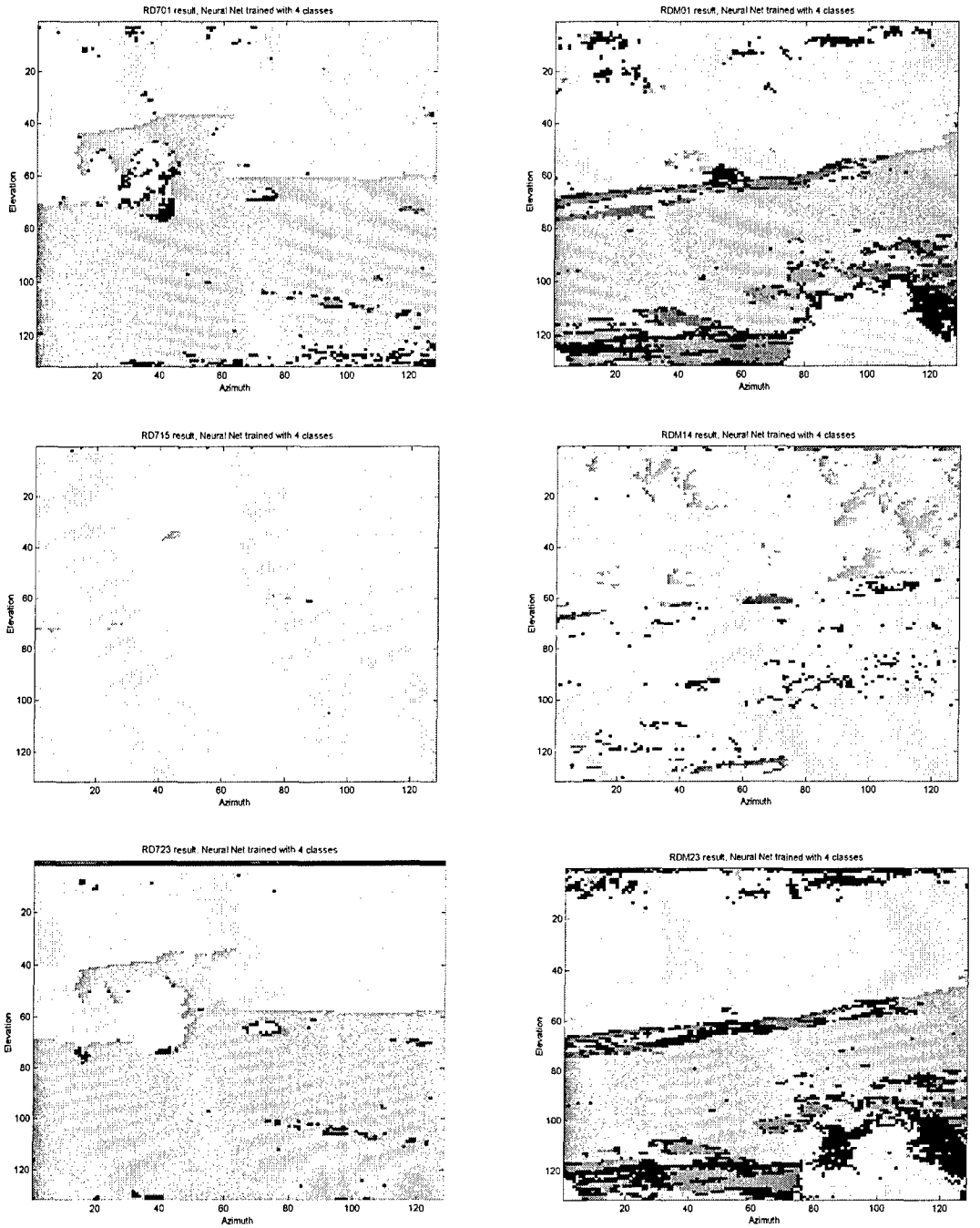

Figure 11. RD7 and RDM segmentation results using a BPNN, trained with only the 4 classes, U.S. target, tree, exposed ground and grass/ground.

We see that the addition of the exposed ground class has clarified the issue. In these renderings, the exposed ground is dark gray to black; however, some pixels still are not classified in these images. We can clearly see the M2 target in the RDM images but the hidden targets in the tree line, the foreign target and camouflaged target are still indistinguishable.

5.3 Segmentation 5 Class Using BPNN

Let us add the foreign target class to the 4 class problem. What follows in Figure 12 are the results for the 5 class segmentation.

Now we have complicated the issue further, adding a 5th class in Figure 12, with the addition of a foreign target.

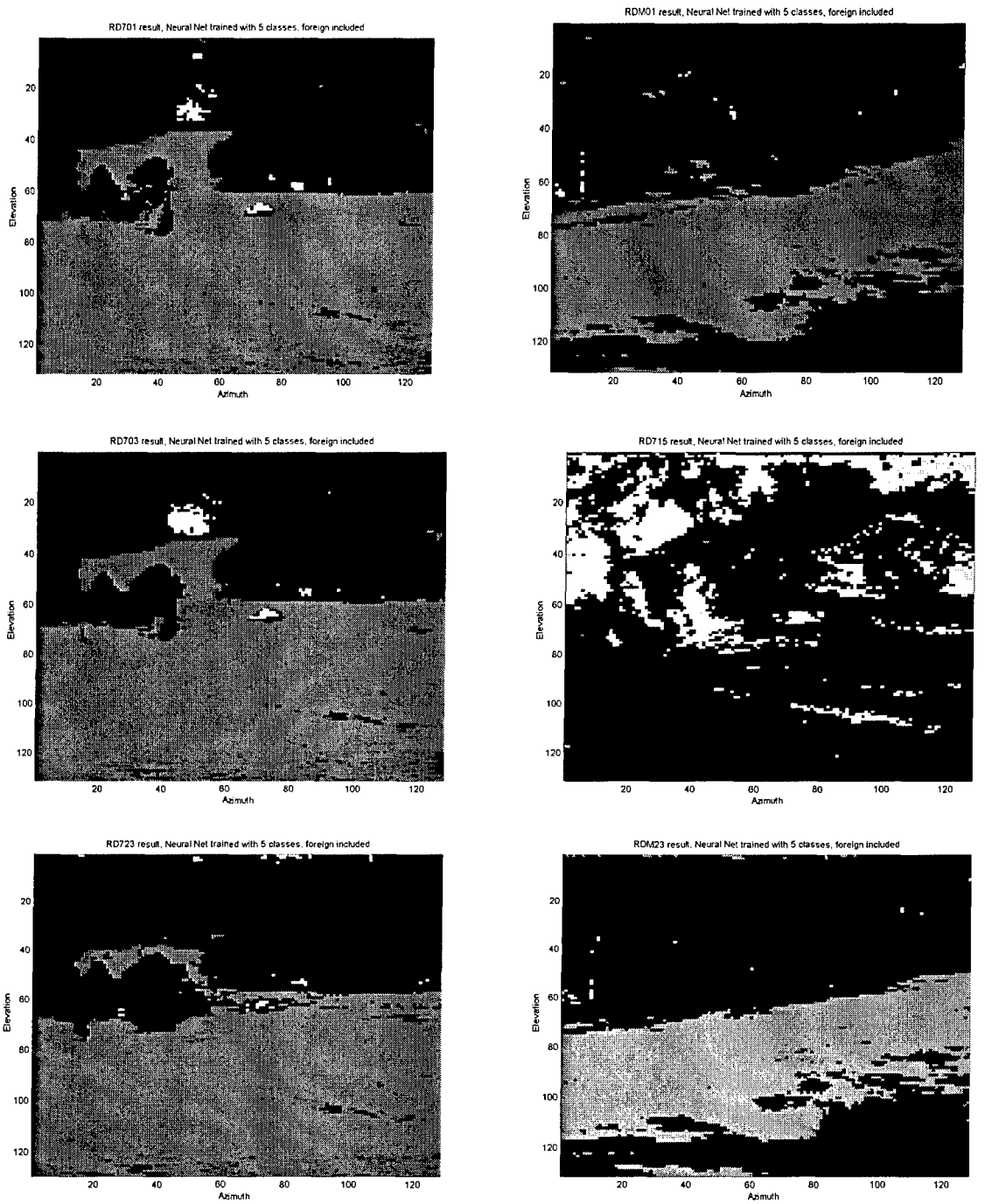

Figure 12. RD7 and RDM segmentation results using a BPNN, trained with 5 classes, U.S. target, foreign target, tree, exposed ground and grass/ground.

We see with the addition of the foreign target (see Figure 3), the trained BPNN with 5 classes begins to exhibit some degradation in performance in segmenting the U.S. targets. Compare the 3 and 4 class cases for the M60 (RD7XXXX) at location x = 72 and y = 64 with the 5 class cases. The temperature inversion and 5 class problem have completely degraded the performance as seen in RD715. We are able though to detect several targets in the RD7 case, especially the late evening images RD723. The region near x = 50 and y = 30 is a mystery but these pixels on closer examination have some similarity to the selected pixels for foreign target.

5.4 Segmentation of 4 Class, Foreign Only

Let us return to a 4 class problem with the foreign target included and without U.S target.

We see that in the foreign target case in Figure 13, we haven't gained anything with regard to segmentation and in fact may have lost some robustness. The figure below is RDM23, a hypercube collected at ~10:00 pm in the evening.

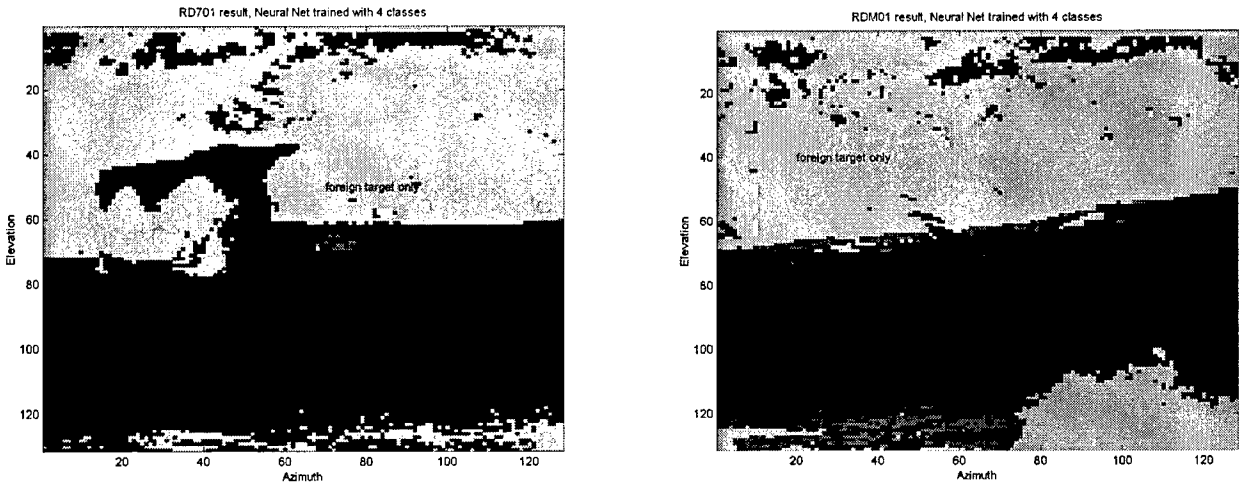

Figure 13. RD7 and RDM segmentation results using a BPNN, trained with 4 classes, foreign target, tree, exposed ground and grass/ground.

Unlike the other trained networks, in Figure 14 we see difficulty in distinguishing the tree line from grass, which may be partly due to the region falling in shadow over the last few hours but moreso, the partitioning of the trained network is now sensitive to these boundaries. You can see the darker gray regions that fill the area between the true tree line and the grass/ground pixels as well as problems with the exposed ground area near the bottom of the image.

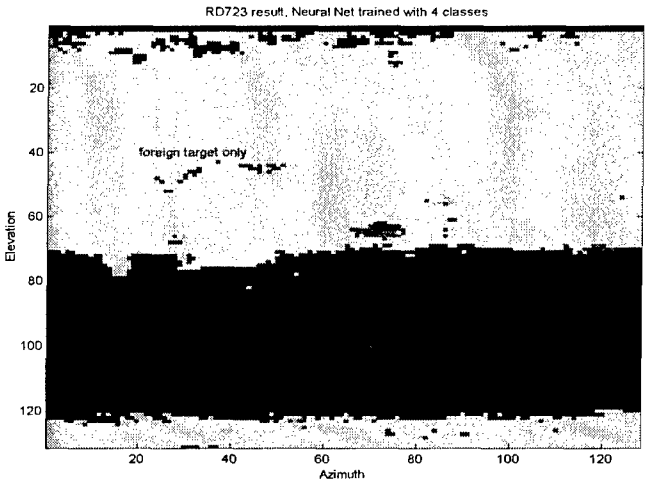

Figure 14. Degraded segmentation performance with foreign target 4 class problem.

5.5 Segmentation Comparison of 4 Class And 5 Class, U.S. and Camouflaged Target

Let us look at the 5 class case segmentation results in Figure 15 where we have added camouflage and U.S. target to the training procedure and compare to the 4 class case with only the camouflage vehicle added.

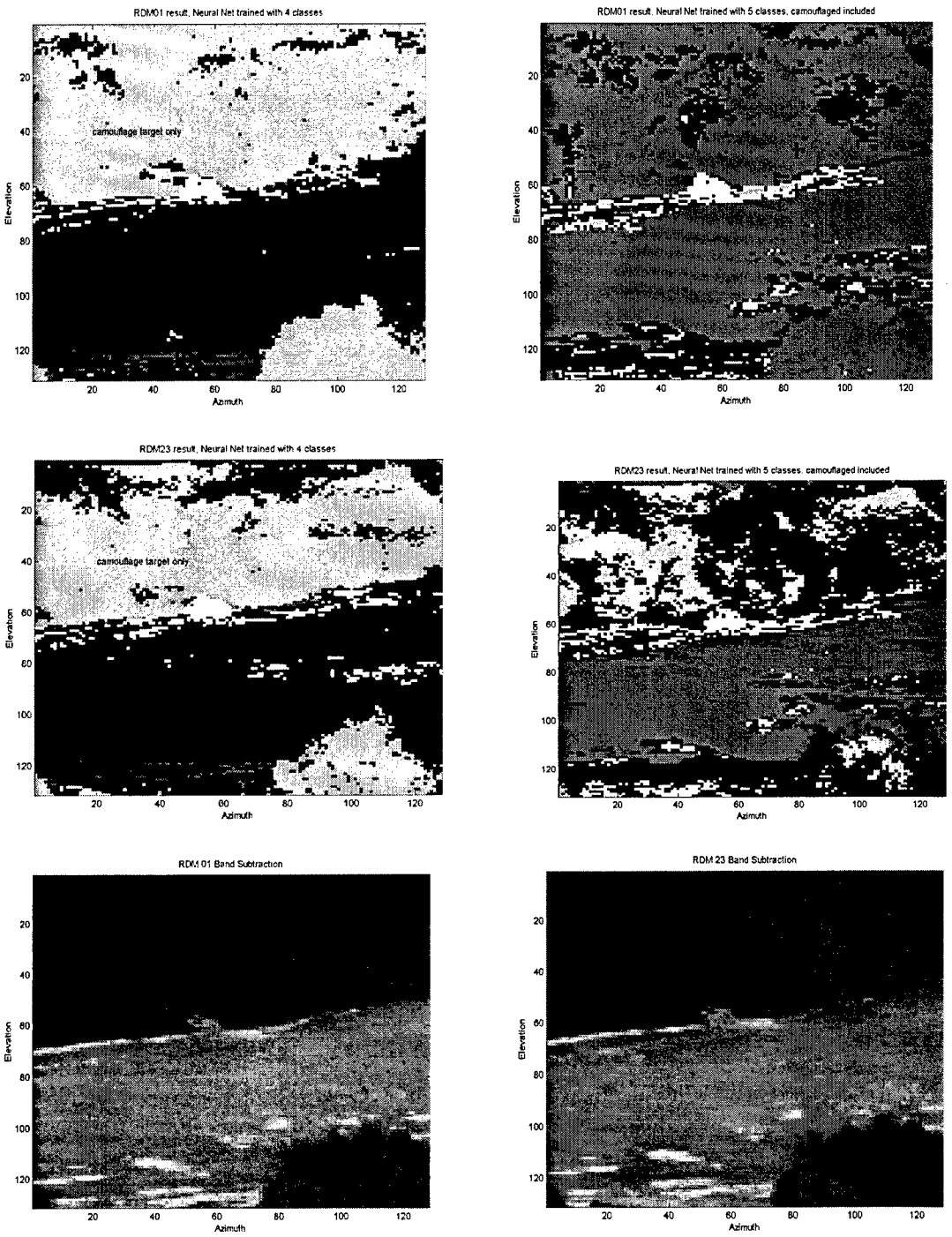

Figure 15. On the left, RD7 and RDM segmentation results using a BPNN, trained with 4 classes, camouflaged target, tree, exposed ground, and grass/ground. On the right, RD7 and RDM segmentation results using a BPNN, trained with 5 classes, U.S. target, camouflaged target, tree, exposed ground, and grass/ground. Band-subtraction images are at the bottom of figure for comparison.

Here we see nearly identical results with the 4 or 5 class trained network and a great improvement over the band-subtraction method for detecting the camouflage vehicle. A segmentation result with an algorithm using spatial techniques could prove very useful. This result is very exciting considering the difficulty in selecting proper training pixels for the camouflage training. We will elaborate on this in the conclusion section.

One more interesting result can be seen in Figure 16 with the 4 class, camouflage trained networks. The RD7 images have targets embedded in the tree line and, therefore, several mixed pixels exist in the image near these targets. Compare Figure 16 with the RD7 case of Figure 12.

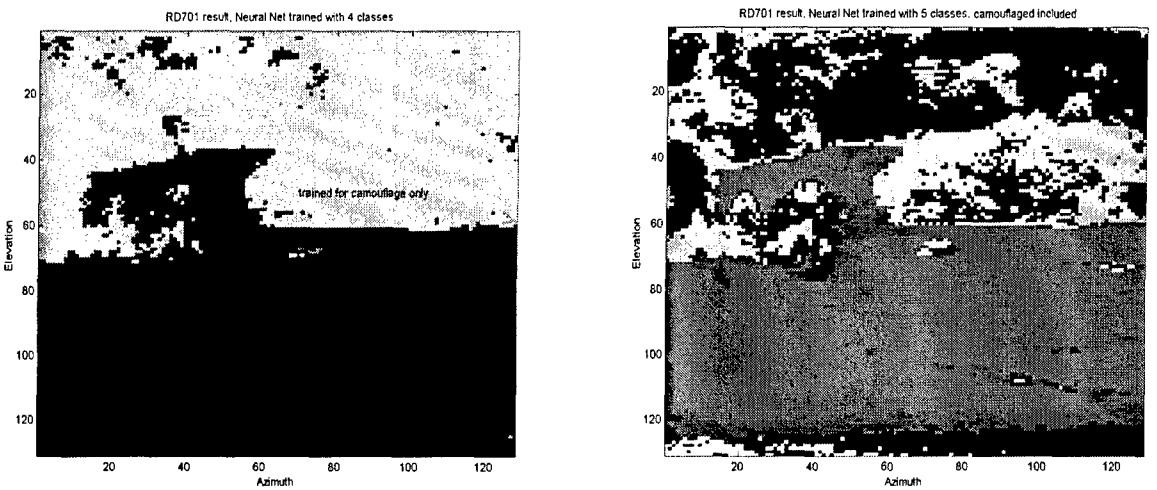

Figure 16. RD7 segmentation results using a BPNN, trained with 4 classes, camouflaged target, tree, exposed ground, and grass/ground, demonstrating the mixed pixel segmentation.

These results demonstrate the mixed pixel nature of the camouflage. Observe the target located at x = 122 and y = 53. We have not been able to detect this target using either U.S. or foreign 4 class trained networks but in the camouflage case it clearly shows up. Also, the pixels near the hidden Russian T-72 tank at x = 84 and y = 55 are not the same that we detected earlier using the foreign case (Figure 13).

5.6 Segmentation of 3 Class, Clutter Only

Figure 17 again demonstrates the great similarity between the target and exposed ground with respect to the parsing of the feature space. Here, only the clutter classes were used and you can readily see the targets despite a threshold applied to the output neuron results. In the RDM case, you see the M2 clearly at x = 2, y = 63.

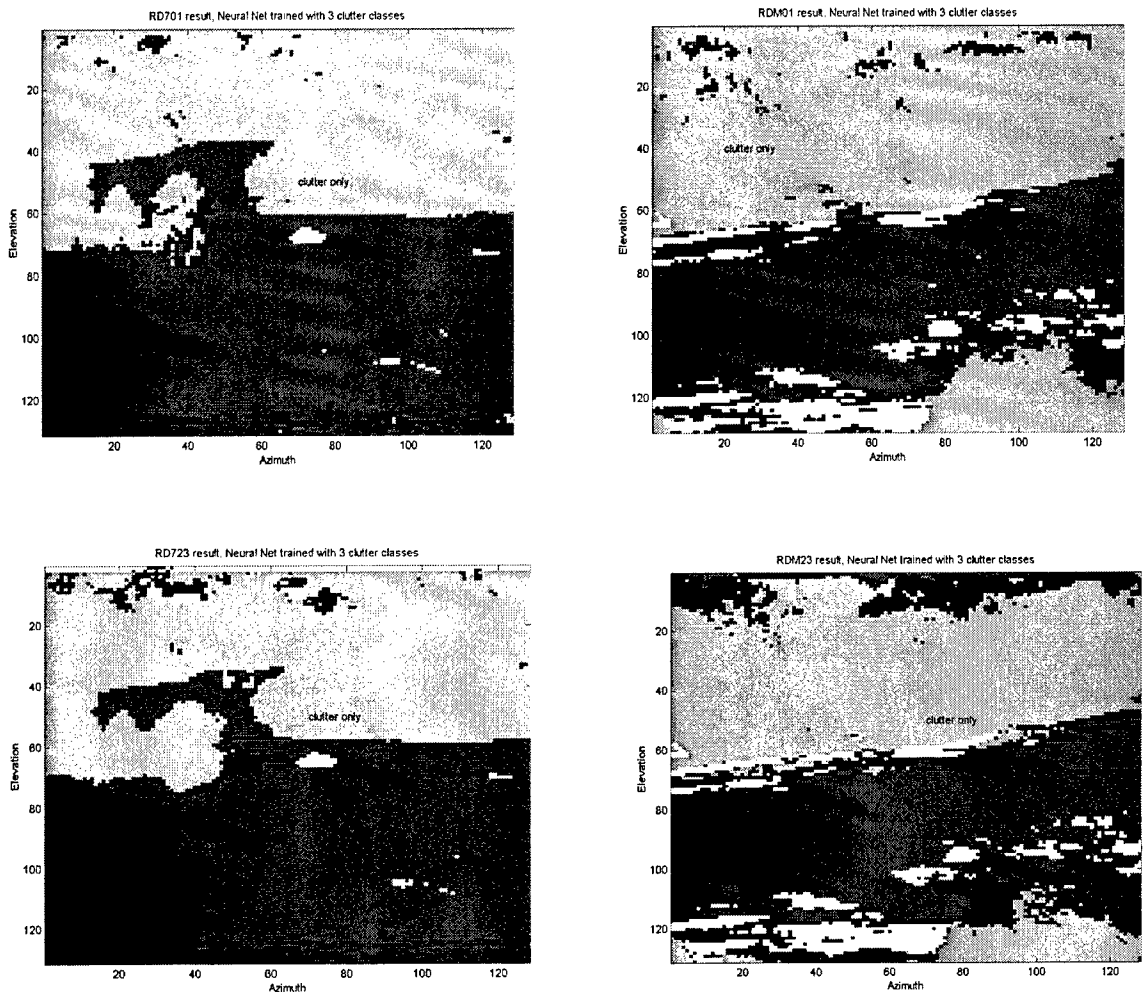

Figure 17. RD7 and RDM segmentation results using a BPNN, trained with 3 classes, tree, exposed ground, and grass/ground.

6. Segmentation Based on Distance Metric

The following sections are examples of other feature methods applied in the 3 class problem with hopes of simplifying and/or improving segmentation. Figure 18 demonstrates several sub-band segmentation results derived with the distance metric. The sub-band region was extracted from 8.7 to 11.3 μm in the relative temperature profile and gave similar results to the distance metrics for full band detection and segmentation result using only the distance metric given by equation (2). Compare the RD7 result with Figure 7.

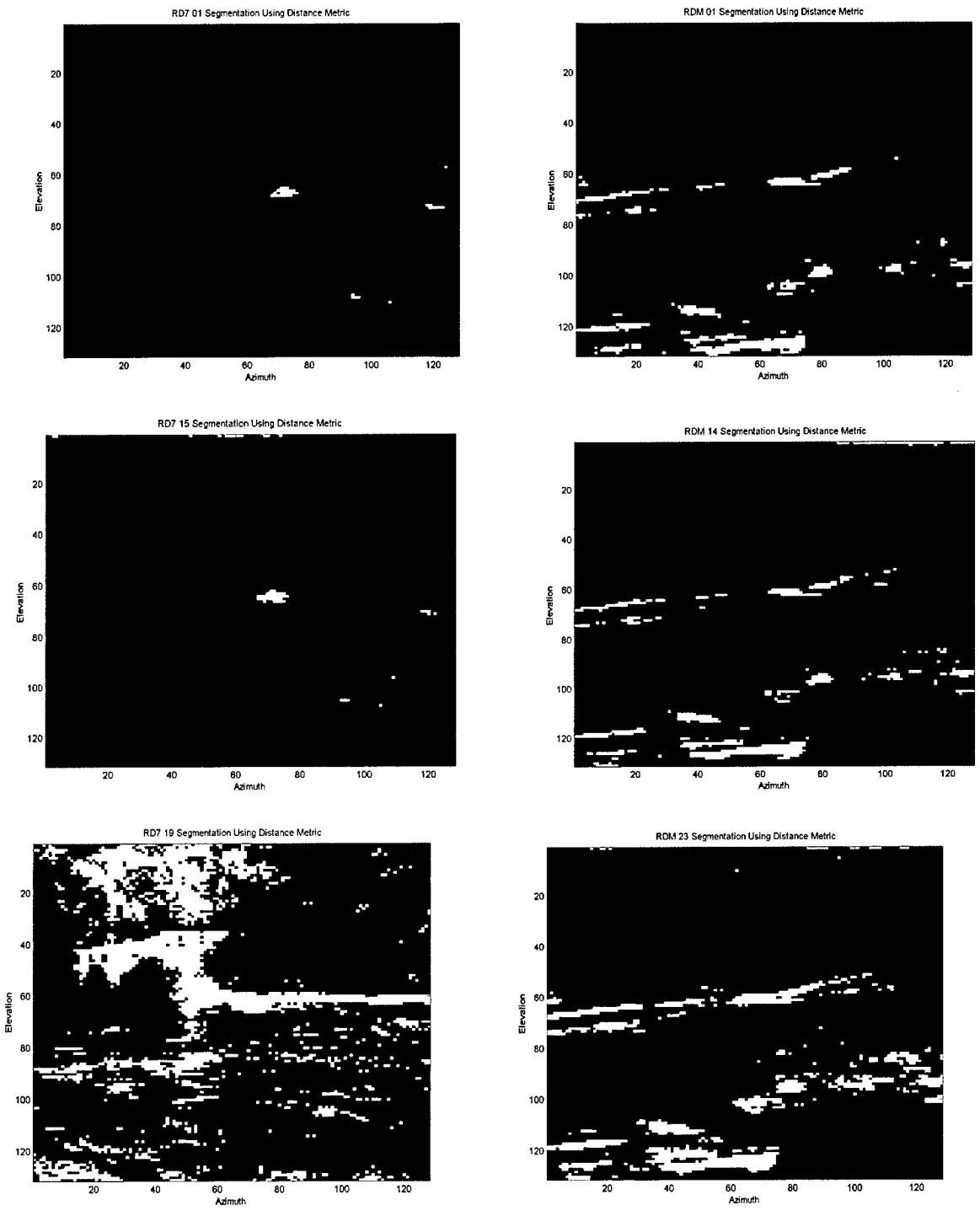

Figure 18. RD7 and RDM segmentation results using a distance metric trained with 3 classes, U.S. target, tree, and grass/ground.

We see the target clearly in the RD7 case as was expected but cannot detect the target in the RDM case. You can see the camouflaged target in the RDM 23, only in the 10:00 pm data collection, but again, the presence of the "target-like" exposed ground class confuses the issue. Clearly, the detrimental effect of the feature's sensitivity to the diurnal cycle resulted in the RD719 image. Typically, a sub-band approach exhibits some immunity to the diurnal changes rather than using the entire spectrum for the simple distance metric.

7. Segmentation Using Broadband and Narrow-Band Features

The broadband feature that was selected uses the wavelengths from 8 to 11 μm. An absolute value of the ratio of the sum of normalized relative temperature values between 8 and 9.5 μm and 9.5 μm to 11.0 μm is the feature. The narrow band features are the differences between a relative temperature at 8.5788 and 8.2706 μm as well as at 8.9920 and 8.8174 μm. These features were selected "ad hoc," by looking over several HSI plots for various classes and by no means have we exhausted the possible choices.

In Figure 19, we can clearly see many of the targets in the simple 3 class, 3-feature case. What is very striking is the target at x = 28 and y = 68 in the RD723 image, a BTR70 that has basically eluded the segmentation techniques used earlier. Again, we see the exposed ground confusing the issue; however in Figure 20, where we have added the fourth class, exposed ground and collected 3 features for each class, we can clearly discriminate the target and exposed ground. This is an exciting result and warrants further investigation because the complexity has been drastically reduced with the 3-feature case.

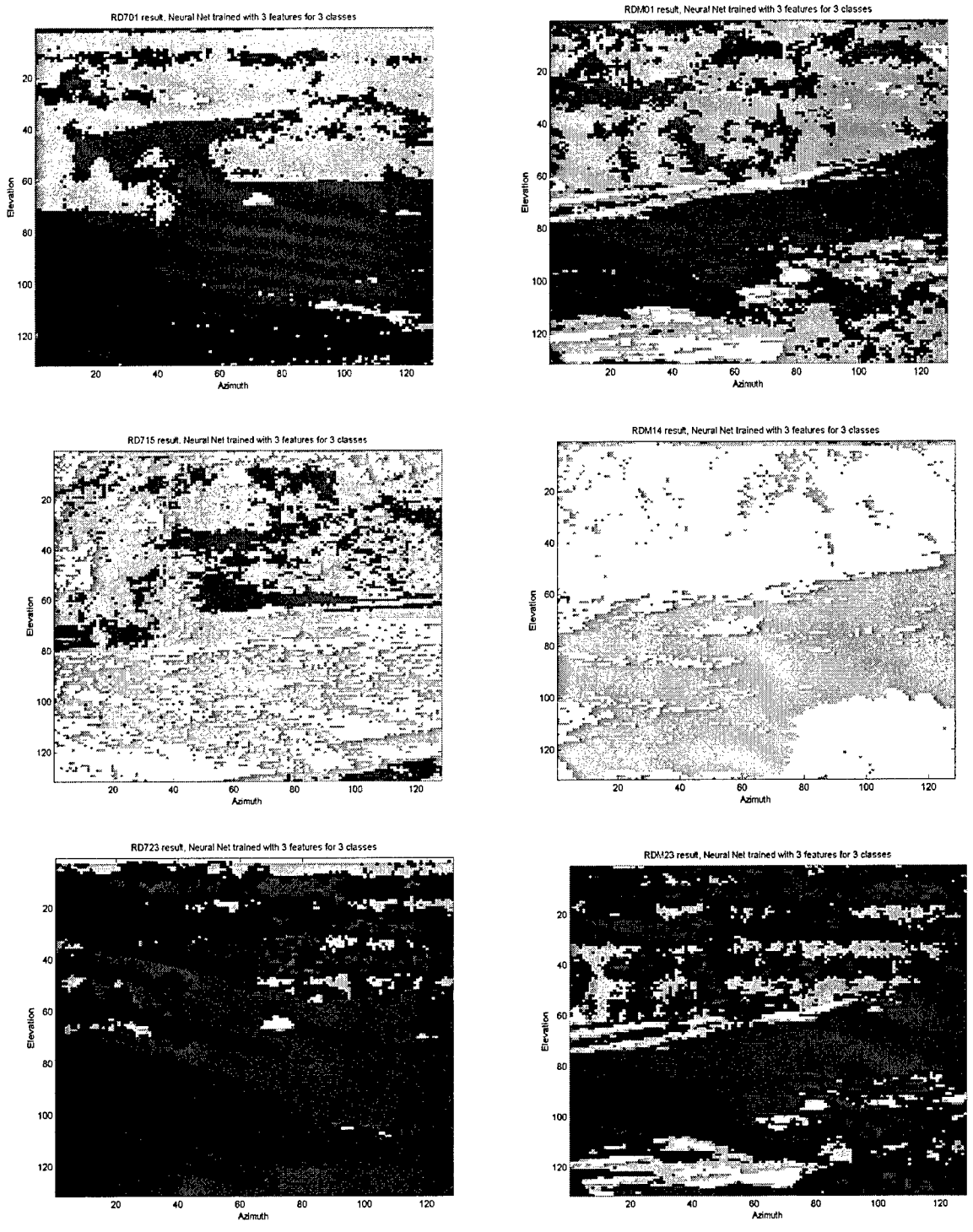

Figure 19. RD7 and RDM segmentation results using a BPNN, trained with 3 classes, U.S. target, tree, and grass/ground. Features are broadband ratio and narrow-band differences.

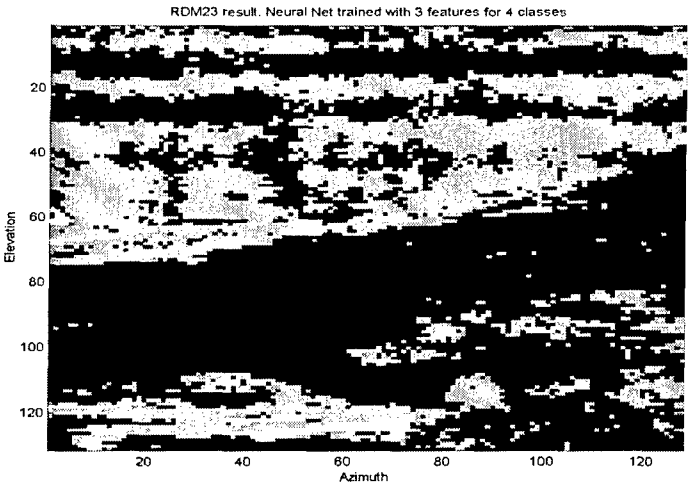

Figure 20. RDM Segmentation result using a BPNN, trained with 4 classes, U.S. target, tree, exposed ground, and grass/ground. Features are broadband ratio and narrow-band differences.

The narrow-band difference features are nearly linear separable for the U.S. target and exposed ground class, as seen in Figure 21.

Figure 21 is a (2-D) of the two narrow-band features for exposed ground and U.S. target. The "crosses" are the 2-D points for the narrow-band features for exposed ground, almost always positive in value, whereas the "stars" represent the 2-D location of the U.S. target narrow-band features, which are typically negative in value.

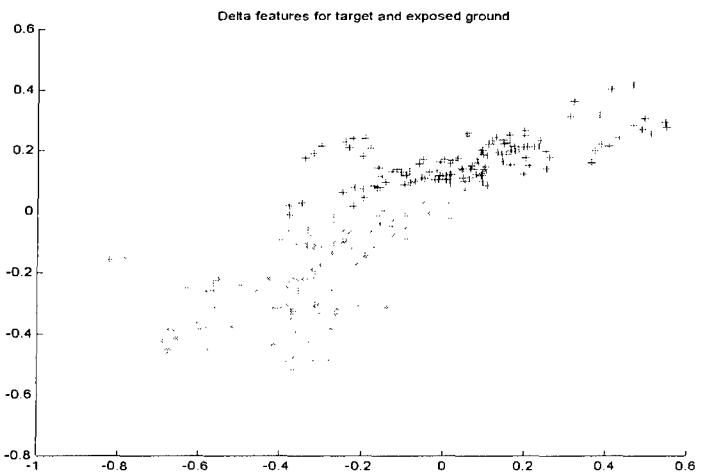

Figure 21. U.S. target and exposed ground narrow band features in 2-D.

8. Principal Components

For the segmentation of full spectrum relative temperature components and the PCA components derived from these same sets. A BPNN was trained using one hidden node for each input node in the case of the full spectrum components and various values for the total hidden nodes were tried with the PCA features. Training was performed using "epoch"-stopping criteria. Further discussion of the networks is not appropriate for this technical report, but see reference [14] for further discussions on neural networks.

The images in Figure 22 are characteristic of segmentation using the BPNN's that were trained with the target principal components and the projections of ground and tree pixels into the target's eigenspace. We see several regions that produce false alarms and therefore any discrimination is lost. It should be mentioned that these images are the result of the target output node class only, and when applying a threshold to these target node outputs, clearer images can be obtained with a small reduction in false alarms. False alarms are in part, due to the sensitivity of the eigenprojection to diurnal changes. A shortcoming of this eigenspace projection procedure is the reliance on one set of eigenvectors. However, an expanded projection method using eigenvectors for the various classes of interest could be considered.

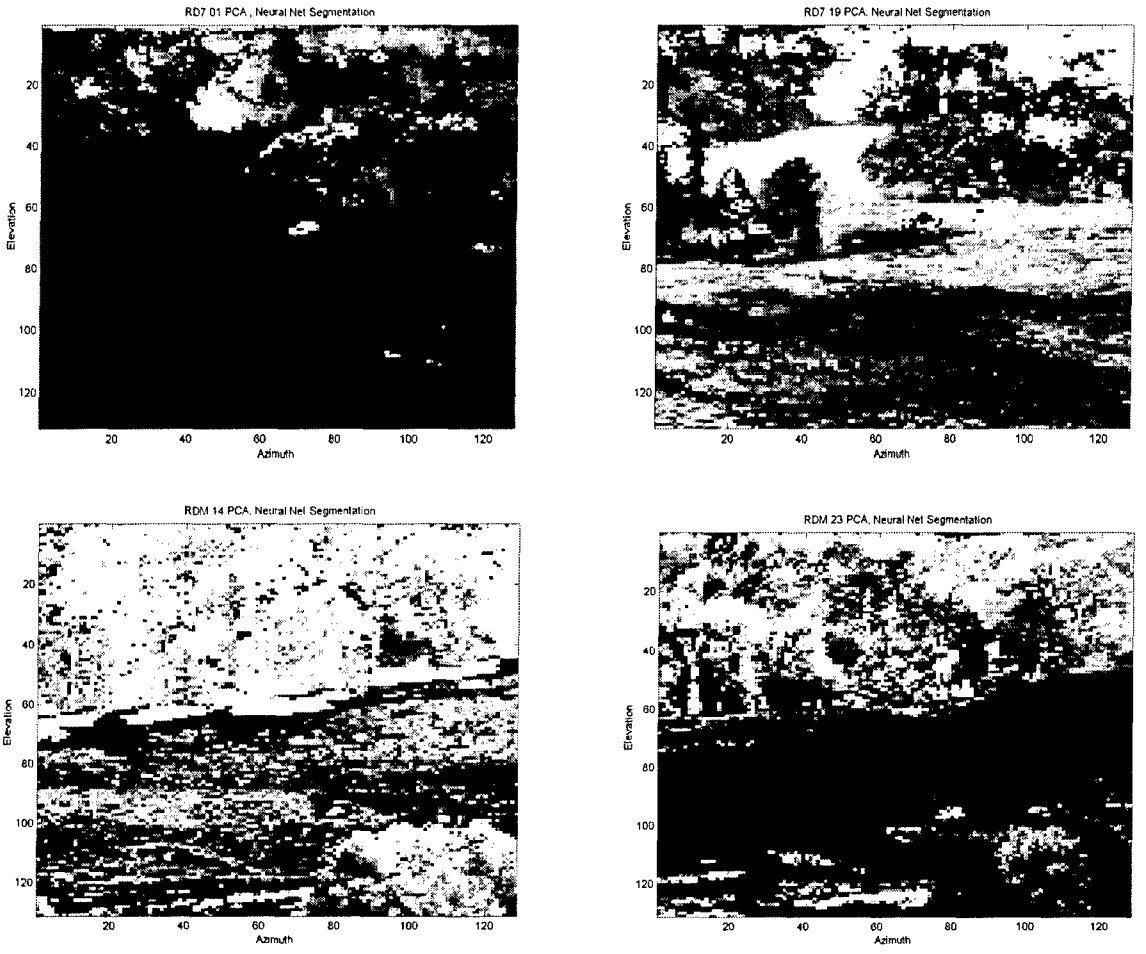

Figure 22. RD7 and RDM segmentation result using a BPNN, trained with 3 classes, U.S. target, tree and grass/ground. Features are projections using 2nd, 3rd and 4th eigenvectors for U.S. target.

9. Diurnal Variation

The following figures are examples of diurnal variations in HSI relative temperature profiles.

As one can readily see in Figure 23, diurnal variations in relative temperature have drastically changed the profiles resulting in the poor performance of the eigenspace projections. Compare these with the means of the training set in Figure 3.

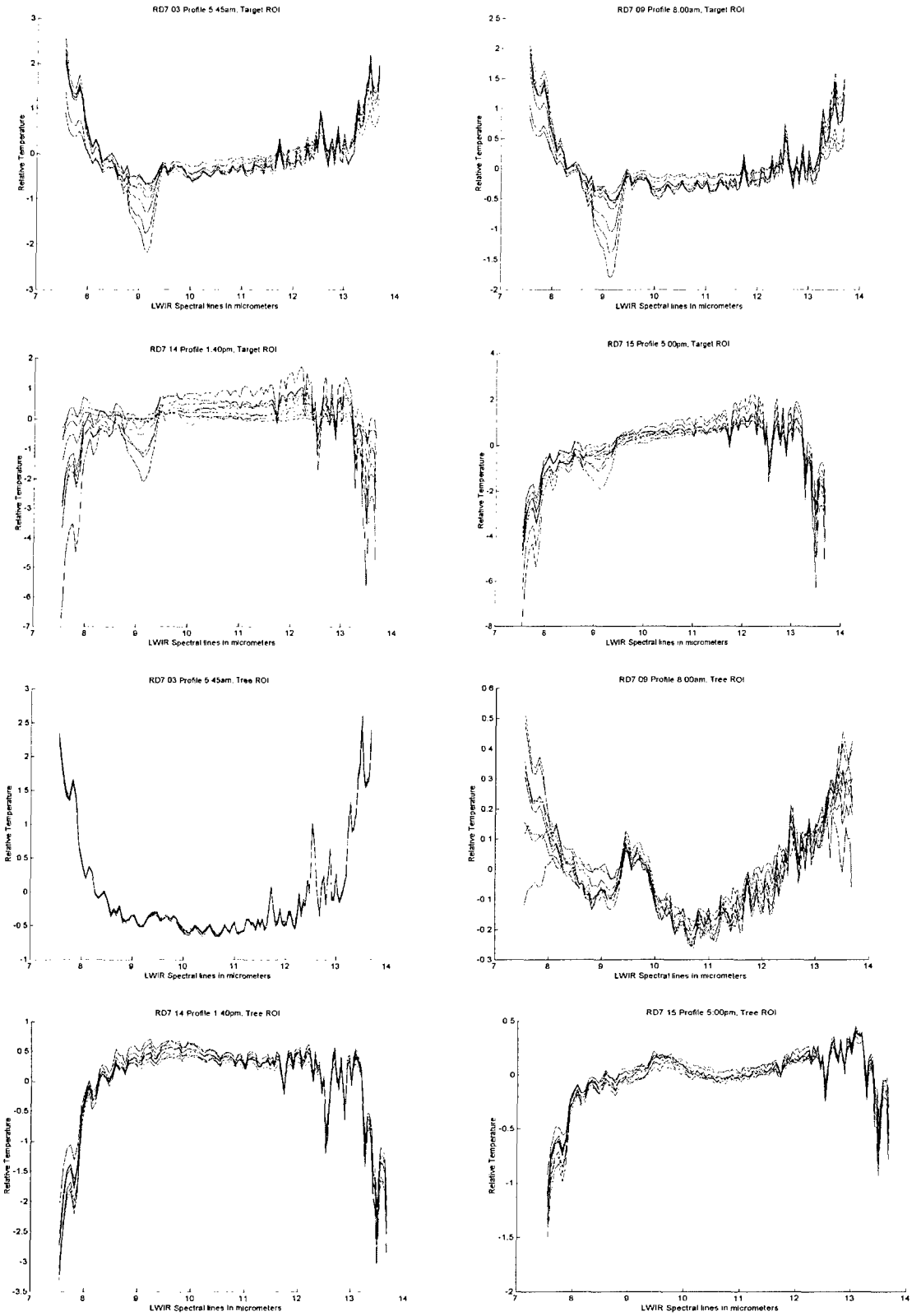

Figure 23. Diurnal variation for U.S. target and tree pixel examples.

Figure 24 is an image representative of the trained neural networks' entire output layer, which we have seen earlier in the paper.

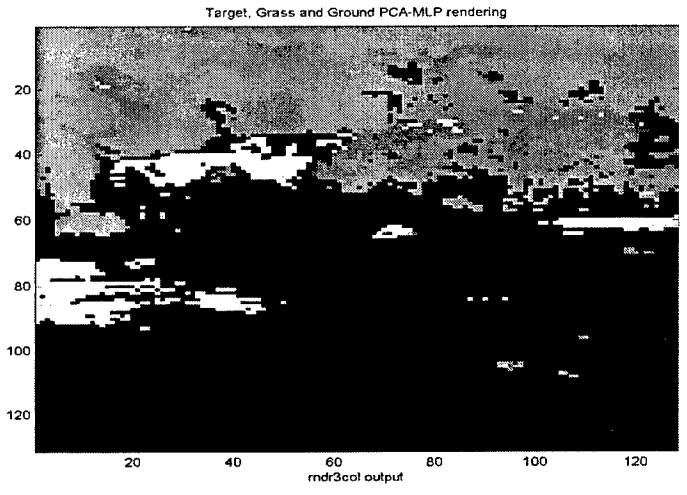

Figure 24. RD7 segmentation depicting some of the richness in target/clutter classes.

This image shows that there is a finer class structure to consider. The brightest areas are target and exposed ground, but we see that the regions of exposed ground are also classified in some cases as the ground/grass. For example, look at [x, y] = [10, 80] in Figure 24. The black areas represent shadowed regions; dark gray regions are ground/grass and trees with light gray regions being predominantly tree locations. Although we have presented results earlier for far more classes, we have by no means exhausted the partitioning of the total classes of clutter and target (mixed pixel) in this image or in the HSI hypercubes. These data were collected in the late morning, which explains the brighter areas of exposed earth centered around [40,40] incorrectly classified as target.

10. Conclusion

The features, either the relative temperature profiles themselves and those derived from using the relative temperature profiles are still in need of further investigation. The broadband and narrow-band features could be extended to include features primarily for class discrimination of the U.S. target, foreign, and perhaps the camouflaged target (mixed pixels). Candidate features include a narrow-band feature derived from taking the difference at 10 and 9 μm, a good feature for U.S. targets (unpublished work), and another narrow-band feature derived from the difference at 11 and 10 μm, which should prove to be an excellent feature for discriminating the foreign class. A broadband feature suggests itself for the foreign class because we see that the relative temperature profile "depression" is shifted and broader for foreign classes. In the foreign target case, we had great difficulty in collecting training features, there simply isn't enough examples in the database. The camouflage case still remains the most difficult although results are promising. Ground truth of our current database is insufficient for the camouflage training collections and must be superior to what is on record for these HSI hypercubes. The closeness of the mixed pixel, exposed ground, and camouflage contribute to the difficulty in selecting a "pure camouflage" pixel for training. During future data collections for camouflage pixels, each pixel associated with the camouflage target must be recorded in the ground truth. It may be of benefit to simply lay camouflage netting on the open ground and collect data at the same time you gather camouflaged target data. Sub-banding looks promising, considering that only 50 spectral bands were used in detecting the camouflaged target in RDM 23 case. Also, this segmentation using the sub-bands was performed using the simple distance metric. A low-complexity classifier architecture coupled with an effective, reduced feature space is the primary goal. Sub-banding and narrow/broadband features fit this notion and hold promise as a method to lend immunity to diurnal changes as well. However, the full spectrum trained nets are superior in segmenting the images. It may be extremely difficult to find salient features that can give good discrimination over the entire diurnal cycle and, therefore, future efforts will be focused on the early morning and late evening cases. PCA may serve as a beneficial feature extraction and compaction method once we restrict the empirical work to the cases previously mentioned, but at this point, there is no advantage to report. Only using the 2nd, 3rd and 4th "projection" is not enough and should be extended. A finer parsing of the various classes in the HSI images, for example, including the class, mixed pixel is expected to improve the detection process, perhaps considering the presence of shadows along the tree line as a specific class may be of benefit as well.

The segmentation architecture has several areas for improvement and exploration. Adaptive techniques and algorithms have been investigated with excellent results [1]. Recurrent networks, feeding the output layers or last few output layer results back to the input layer, would bring a spatial reference to the segmentation. Codebooks for the various classes could be constructed contributing to the segmentation options and utility. Finally, modeling mixed pixels may allow one to artificially extend the camouflage database, with the hope of improving segmentation.

11. References

[1] H. Kwon, S. Der and N.M. Nasrabadi, "An Adaptive Hierarchical Segmentation Algorithm Based on Quadtree Decomposition For Hyperspectral Imagery," IEEE International Conference on Image Processing, ICIP 2000 Vancouver, Canada, Sept., 10-13 2000

[2] M. Sola and D. Beekman, "Hyperspectral Algorithm Development for Army Applications," Ground Target Modeling and Validation Conference, Houghton MI, August 1999

[3] H. Kwon, S. Der and N.M. Nasrabadi, "Use of hyperspectral imagery for material classification in outdoor scenes," in Proceedings of the SPIE, vol. 3804, (Denver ,CO), pp. 104-115, 1999.

[4] J. Harsanyi and C Chang, "Hyperspectral Image Classification and Dimensionality Reduction: An Orthogonal Subspace Projection Approach," IEEE Transactions on Geoscience and Remote Sensing, vol. 32, no. 4, July 1994 ,pp 779-785

[5] P. Rauss, J Daida and S Chaudhary, "Classification of Spectral Imagery Using Genetic Programming," GECCO-2000: Proceedings of the Genetic and Evolutionary Computation Conference, July 10 - 12, 2000, Las Vegas, Nevada. San Francisco: Morgan Kaufmann Publishers.

[6] C Chang, Q. Du, T Sun and M. Althouse, "A Joint Band Prioritization and Band-Decorrelation Approach to Band Selection for Hyperspectral Image Classification," IEEE Transactions on Geoscience and Remote Sensing,", vol. 37, no. 6, November 1999, pp 2632-2641

[7] C. Schwartz, J. Cederquist and D. Twede, "Detection of Low Contrast CC&D Targets Using Hyperspectral Infrared Image Data," Proc. Of IRIS Specialty Group on Camouflage, Concealment and Deception, Monterey, CA 1997

[8] P.J. Ready and P.A. Wintz, "Information Extraction, SNR improvement, and data compression in multispectral imagery," IEEE Trans. Commun., vol,21 pp. 1123-1130, 1973

[9] F. Shin and D. Kil, "Pattern Recognition and Prediction with Applications to Signal Characterization," American Institute of Physics, Woodbury , NY (1996)

[10] J. Ryzin, "Classification and Clustering," Academic Press, New York (1977)

[11] K. Ng and Lippmann R., "Practical characteristics of neural network and conventional pattern classifiers," Advances in Neural Information Processing Systems 1991, San Mateo Ca.

[12] K. Fukunaga, "Introduction to Statistical Pattern Recognition," 2nd Edition Academic Press, San Diego, 1990

[13] R. O. Duda and P.E. Hart, "Pattern Classification and Scene Analysis," John Wiley and Sons, Inc., 1973

[14] S. Haykin, "Neural Networks, A Comprehensive Foundation," Macmillan Publishing Company, New Jersey,1994